J|A|C|S
ARTICLES
Published on Web 02/03/2005

Systematic Study of the Structure−Property Relationship of a Series of Ferrocenyl Nonlinear Optical Chromophores

Yi Liao,[†] Bruce E. Eichinger,[†] Kimberly A. Firestone,[†] Marnie Haller,[‡] Jingdong Luo,[‡] Werner Kaminsky,[†] Jason B. Benedict,[†] Philip J. Reid,[†] Alex K-Y Jen,[†,‡] Larry R. Dalton,[†] and Bruce H. Robinson*[,†]

Contribution from the Department of Chemistry and Department of Materials Science and Engineering University of Washington, Seattle, Washington 98195-2120

Received August 23, 2004; E-mail: robinson@chem.washington.edu

Abstract: A series of novel nonlinear optical (NLO) chromophores **1**−**4** incorporating the ferrocenyl (Fc) group as an electron donor and 2-dicyanomethylene-3-cyano-4-methyl-2,5-dihydrofuran (TCF) derivatives as electron acceptors are presented. The use of a constant Fc donor and varied acceptors and bridges makes it possible to systematically determine the contribution of the conjugated bridge and the acceptor strength to chromophore nonlinear optical activity. The X-ray crystal structures of all four chromophores allow for the systematic investigation of the structure−property relationship for this class of molecules. For example, the crystal structures reveal that both cyclopentadienyl groups in the ferrocenyl donor contribute to the electron donating ability. The first-order hyperpolarizabilities β of these chromophores, measured by hyper-Rayleigh scattering (HRS) relative to *p*-nitroaniline are reported. These β values are compared to those calculated by density functional theory (DFT). The excellent agreement between the theoretical and experimental β values demonstrates that a linear relation exists between the hyperpolarizability and the bond length alternation. An electrooptic coefficient, r_{33}, of ∼25 pm/V at 1300 nm, for compound **4**, incorporated into a polymer matrix, is competitive with organic chromophores. Moreover, this r_{33} is more than 30 times larger than the previously reported value for an organometallic chromophore in a poled polymer matrix. This work not only underscores the potential for Fc donor moieties, which have been underutilized, but also demonstrates that experimental characterization and theoretical simulations are now congruent, viable methods for assessing potential performance of NLO materials.

Introduction

Second-order nonlinear optical chromophores with a ferrocenyl (Fc) group as the electron donor have been of considerable interest.[1] The molecular hyperpolarizability of Fc chromophores has been studied by electric field-induced second harmonic generation (EFISH) and hyper-Rayleigh scattering (HRS).[2] A Fc chromophore with $\mu\beta$ as large as 11200×10^{-48}esu has been achieved.[2b] The potentially attractive NLO properties are coupled with good thermal and photochemical stability[3] and redox switching ability.[4] Moreover, the Fc chromophore is bulkier than typical organic NLO donor groups, making the Fc moiety a donor with distinct properties, resulting in novel chromophore architectures.

Wright et al.[5] studied second harmonic generation of main-chain, side-chain, and guest−host polymers of Fc chromophores. A second harmonic intensity (SHG) 4 times that of y-cut quartz crystal was measured. Marder et al.[6] studied the electrooptic effect of a Fc chromophore in a polymer matrix. Specifically, 1-ferrocenyl-4-*E*,*E*(4-nitrophenyl)butadiene was doped in poly(methyl methacrylate) (PMMA) at 2% molar loading; after poling at 100 MV/m the resulting film demonstrated an $r_{33} = 0.8$ pm/V as measured at 820 nm. This is the first and only report of an r_{33} for an organometallic chromophore in a polymer matrix. Since then, presumably because of such poor performance, the Fc moiety has not been actively used in electrooptical materials.

[†] Department of Chemistry.
[‡] Department of Materials Science and Engineering.

(1) Di Bella, S. *Chem. Soc. Rev.* **2001**, *30*, 355. Barlow, S.; Marder, S. R. *Chem. Commun.* **2000**, 1555. Heck, J. Dabek, S.; Meyer-Friedrichsen; Wong, H. *Coord. Chem. Rev.* **1999**, *190*−*192*, 1217. Verbiest, T.; Houbrechts, S.; Kauranen, M.; Clays, K.; Persoons, A. *J. Mater. Chem.* **1997**, *7*, 2175. Long, N. J. *Angew. Chem., Int. Ed. Engl.* **1995**, *34*, 21. Kanis, D. R.; Ratner, M. A.; Marks, T. J. *Chem. Rev.* **1994**, *94*, 195.
(2) For example: (a) Janowska, I.; Zakrzewski, J.; Nakatani, K.; Delaire, J. A.; Palusiak, M.; Walak, M.; Scholl, H. *J. Organomet. Chem.* **2003**, *675*, 35. (b) Alain, V.; Blanchard-Desce, M.; Chen, C.; Marder, S. R.; Fort, A.; Barzoukas, M. *Synth. Met.* **1996**, *81*, 133. (c) Blanchard-Desce, M.; Runser, C.; Fort, A.; Barzoukas, M.; Lehn, J.-M.; Bloy, V.; Alain, V. *Chem. Phys.* **1995**, *199*, 253. (d) Calabrese, J. C.; Cheng, L. T.; Green, J. C.; Marder, S. R.; Tam, W. *J. Am. Chem. Soc.* **1991**, *113*, 7227.
(3) Rosenbulm, M. *Chemistry of the Iron Group Metallocenes*; Weiley: New York, 1965. Harwood, J. W. *Industrial Applications of Organometallic Compounds*; Reinhold: New York, 1963. Johnson, J. C., Jr. *Metallocene Technology*; Noyes Data Corp.: Park Ridge, NJ, 1973. Neuse, E. W.; Woodhouse, J. R.; Montaudo, G.; Puglis, C. *Appl. Organomet. Chem.* **1988**, *2*, 53.
(4) (a) Malaun, M.; Reeves, Z. R.; Paul, R. L.; Jeffery, J. C.; McCleverty, J. A.; Ward, M. D.; Asselberghs, I.; Clays, K.; Persoons, A. *Chem. Commun.* **2001**, 49. (b) Asselberghs, I.; Clays, K.; Persoons, A.; McDonagh, A. M.; Ward, M. D.; McCleverty, J. A. *Chem. Phys. Lett.* **2003**, *368*, 408. (c) Marder, S. R.; Cheng, L. T.; Tiemann, B. G.; Friedli, A. C.; Blanchard-Desce, M.; Perry, J. W.; Skindhoej, J. *Science* **1994**, *263*, 511.
(5) Wright, M. E.; Toplikar, E. G.; Lackritz, H. S.; Kerney, J. T. *Macromolecules* **1994**, *27*, 3016. Wright, M. E.; Toplikar, E. G.; Kubin, R. F.; Seltzer, M. D. *Macromolecules* **1992**, *25*, 1838.
(6) Alain, V.; Fort, A.; Barzoukas, M.; Chen, C. T.; Blanchard-Desce, M.; Marder, S. R.; Perry, J. W. *Inorg. Chim. Acta* **1996**, *242*, 43.

10.1021/ja0449123 CCC: $30.25

Growing noncentrosymmetric crystals is another approach to achieve electrooptically active materials. Most published crystal structures of Fc chromophores[2a,4a,7,8] have centrosymmetrical structures. When coupled to strong acceptors, the chromophores tend to pack antiparallel because of the strong dipole−dipole interactions. Occasionally a ferrocenyl-based chromophore will generate a crystal structure that is noncentrosymmetric;[9] however, such occurrences are rare. Therefore, doping or linking Fc chromophores into a polymer matrix followed by poling to form an NLO active material presents a more practical and reliable approach to realizing noncentrosymmetric NLO materials.

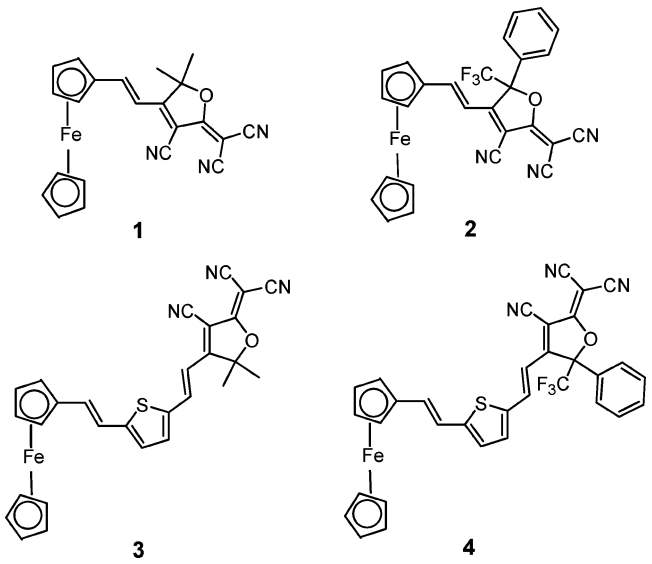

In addition to the electron donor, the electron acceptor can have a pronounced effect on the molecular hyperpolarizability. In recent years, a number of strong electron acceptors have been developed to increase the hyperpolarizability of NLO chromophores. Among those are the 2-dicyanomethylene-3-cyano-4-methyl-2,5-dihydrofuran (TCF) type acceptors. Chromophores containing the TCF acceptor have been used to achieve sub-1-volt halfwave voltage polymeric electrooptic modulators[10] and an r_{33} electrooptic coefficient higher than 45 pm/V.[11] Mating acceptors with distinct properties to the Fc donor may provide a new strategy to develop even better NLO materials. Therefore, we present the synthesis, crystal structures, and experimental and theoretical characterization of some Fc chromophores coupled to the TCF-type acceptor, **1**−**4**. This series of chromophores is suitable for isolating the effects of increasing acceptor strength and π bridge length conjugation. The effects of longer π bridges have been studied extensively.[2] However, it is not straightforward to design a series of model compounds to study the effects of acceptor strength. First, to clearly compare the acceptor strength, the two acceptors must have similar structures. Also, to isolate the acceptor effect from the bridge effect, it is preferred that the functional group that increases the acceptor strength is not conjugated to the π system. Third, the effects should be strong and unambiguous. Comparing the electron-withdrawing ability of CF_3PhTCF acceptor **6** with that of the TCF acceptor **5** (see below), it is seen that **6** is enhanced by a nonconjugated CF_3 group. These two acceptors, **5** and **6**, fulfill all three requirements and are good models for studying the acceptor effect. The electrooptic properties of amorphous polycarbonate doped with **3** and **4** is also studied for comparison.

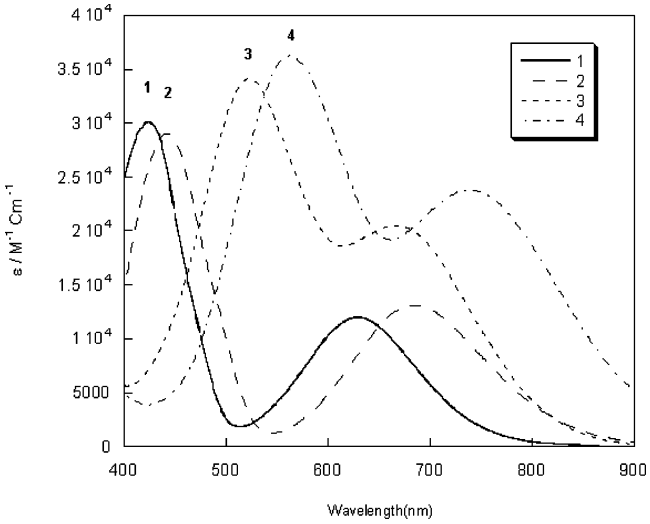

Figure 1. UV−vis spectra of **1**−**4**.

Results and Discussion

Synthesis. Chromophores **1**−**4** were synthesized as shown in Scheme 1. The TCF acceptor **5** was synthesized following literature methods.[12] Its derivative acceptor **6**, CF_3PhTCF, was prepared by a three-step synthesis, illustrated in Scheme 1. Compound **6** had been synthesized by He, et al.[13] However, we were not able to repeat the last step of their procedure. Instead, we utilized a microwave-assisted condensation method developed by Liu et al.[11] and used lithium ethoxide instead of sodium ethoxide as the catalyst. This microwave-assisted synthesis produced **6** with 42% yield. The synthesis of Fc compounds **7** and **8** followed literature methods except that diethyl-thiophenyl-phosphonate instead of triphenyl-thiophenyl-phosphonium bromide was used as the starting material in the Wittig reactions.[8] Knoevenagel condensation of the aldehydes with the acceptors yielded the chromophores. The condensation of the Fc aldehydes with CF_3PhTCF, acceptor **6**, in ethanol was extremely efficient. No base or heating was necessary to accelerate the reaction.

UV−Visible Absorbance Spectra. The spectra of the Fc chromophores show two strong transitions in the UV−vis region (as shown in Figure 1). We found that increasing either the acceptor strength or the length of the π bridge caused a red-shift for both the higher energy transition (HE) band and the lower energy transition (LE) band. However, the strength of

(7) For example: Shin, D. M.; Lee, I. S.; Chung, Y. K. *Eur. J. Inorg. Chem.* **2003**, *12*, 2311. Chiffre, J.; Averseng, F.; Balavoine, G. G. A.; Daran, J.-C.; Iftime, G.; Lacroix, P. G.; Manoury, E.; Nakatani, K. *Eur. J. Inorg. Chem.* **2001**, *9*, 2221. Balavoine, G. G. A.; Daran, J.-C.; Iftime, G.; Lacroix, P. G.; Manoury, E.; Delaire, J. A.; Maltey-Fanton, I.; Nakatani, K.; Di Bella, S. *Organometallics* **1999**, *181*, 21.
(8) Thomas, K. R. J.; Lin, J. T.; Wen, Y. S. *J. Organomet. Chem.* **1999**, *575*, 301.
(9) Green, M. L. H.; Marder, S. R.; Thompson, M. E.; Bandy, J. A.; Bloor, D.; Kolinsky, P. V.; Jones, R. J. *Nature* **1987**, *330*, 360.
(10) Shi, Y.; Zhang, C.; Zhang, H.; Bechtel, J. H.; Dalton, L. R.; Robinson, B. H.; Steier, W. H. *Science* **2000**, *288*, 119.
(11) Liu, S.; Haller, M. A.; Ma, H.; Dalton, L. R.; Jang, S.-H.; Jen, A. K.-Y. *Adv. Mater.* **2003**, *15*, 603.
(12) Melikian, G.; Rouessac, F. P.; Alexandre, C. *Synth. Commun.* **1995**, *25*, 3045.
(13) He, M.; Leslie, T. M.; Sinicropi, J. A. *Chem. Mater.* **2002**, *14*, 2393.

Scheme 1

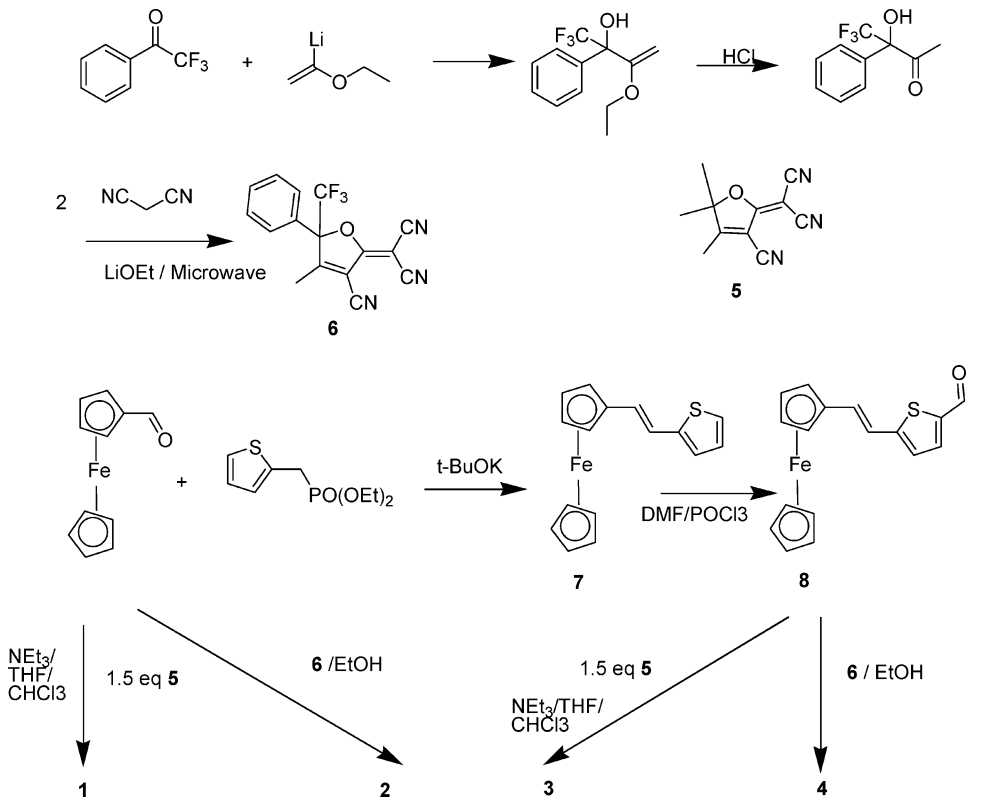

Table 1. UV−Vis Data on the HE and LE Bands of **1**−**4** (in chloroform)

compound	λ_{max} [nm] (ϵ [M^{-1} cm^{-1}])	$h\nu$ [eV]
1	424 (30058), 630 (11908)	2.92, 1.97
2	442 (29001), 684 (13090)	2.81, 1.81
3	522 (34107), 664 (20464)	2.38, 1.87
4	562 (36225), 738 (23760)	2.21, 1.68

the acceptor shifts the LE more than the HE, while the length of the π bridge shifts the HE more than the LE. This behavior is clearly demonstrated by comparing **2** with **3** (Table 1). Chromophore **2** has a stronger acceptor, while **3** has a longer conjugated bridge. UV−vis spectra showed that the λ_{max} of the HE band of **2** is 79 nm shorter than that of **3**, while for the LE band, λ_{max} of **2** is 21 nm longer than that of **3**. When the conjugated bridge gets longer, the acceptor does not preferentially shift the LE more than the HE. From **1** to **2**, the red-shift of the LE band (0.16 ev) is about 50% more than that of the HE band (0.11 ev), while from **3** to **4**, the red-shift of the LE band (0.19 ev) is only a little larger than that of the HE band (0.17 ev). The UV−vis data of **1**−**4** are listed in Table 1, and the spectra are in Figure 1.

As previously mentioned, compounds **1**−**4** are excellent model compounds for the study of the effect of both the acceptor and the conjugated system. Different models have been proposed to assign the transitions and explain the effects of acceptors and conjugated bridges[2d,14] on NLO activity. A recent model developed by Barlow et al.[15] assigns the LE band to a transition between a set of degenerate HOMOs and a LUMO, and the HE band to a transition between an occupied orbital labeled π and the LUMO. The π orbital is formed from a combination of the highest occupied cyclopentadienyl orbital and the highest occupied π bridge orbital. The LUMO is largely localized on the acceptor with a small contribution from the bridge; thus, it represents the characteristics of the acceptor. The HOMOs correspond to the nonbonding nearly degenerate $d_{z^2}/d_{x^2-y^2}/d_{xy}$ orbitals of the metal. The idealized model predicts that changing acceptor strength will affect the HE and LE bands equally, whereas changing the conjugated bridge will affect only the HE.

Our results deviate from the prediction of the idealized model. The interaction between the conjugated bridge and the metallocene and the interaction between the acceptor and the conjugated bridge must both be considered to correctly predict the effects. When the acceptor strength increases, the energy of the π orbital will decrease with the decrease of the LUMO, while the HOMO will remain the same. Therefore, the decrease of the energy gap between the LUMO and the π orbital will be smaller than between that of the LUMO and HOMO. That is the reason that the acceptor strength affects the LE band more than the HE band. When the length of the conjugated bridge increases, the acceptor will affect the π orbital relatively less, and the two gaps (HOMO−LUMO and π-LUMO**)** will become closer. Simple Hückel arguments predict that an increase in conjugation length will increase the energy of the π orbital. Because of the interactions of the bridge with the ferrocene, this will modestly increase the HOMO. Given the electron-donating nature of the thiophene bridge, the interaction between the bridge with the acceptor will also increase the LUMO which is mostly localized on the acceptor. The combination of these two effects will not significantly change the gap between the LUMO and the HOMO. Therefore, changing the conjugated

(14) Kanis, D. R.; Ratner, M. A.; Marks, T. J. *J. Am. Chem. Soc.* **1990**, *112*, 8203. Kanis, D. R.; Ratner, M. A.; Marks, T. J. *J. Am. Chem. Soc*. **1992**, *114*, 10338.

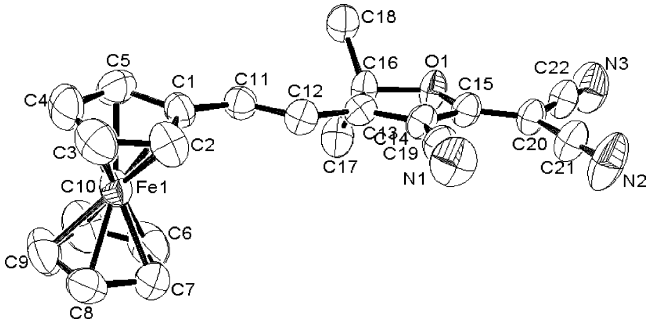

Figure 2. ORTEP labeling (50%) of **1**. (CCDC 249699. Some selected bond distances are listed in ref 16.)

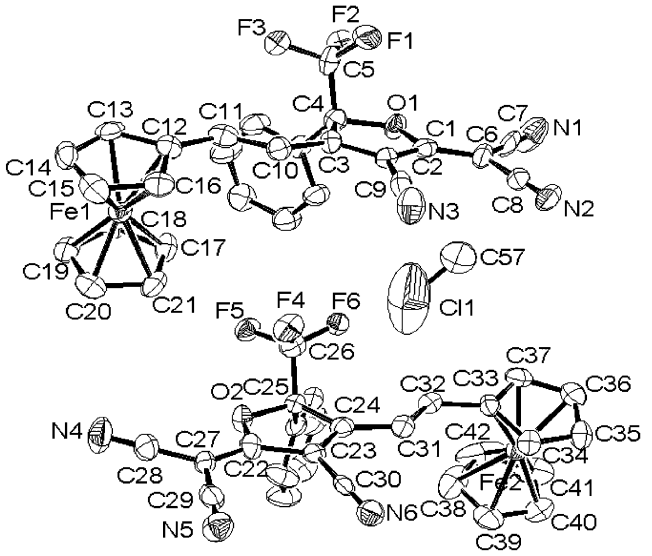

Figure 3. ORTEP labeling (50%) of **2**. (CCDC 249701. Some selected bond distances are listed in ref 16.)

tobridge structure or length will affect the HE band more than the LE band.

Crystal Structures. Single-crystal X-ray diffraction provides a reliable measure of molecular structure, providing information for the study of the structure−property relationship and intermolecular interactions among chromophores. Crystals of all four chromophores were obtained by slow diffusion of a heptane layer into a concentrated solution of the corresponding chromophore in dichloromethane. All four compounds form centrosymmetric crystal structures. Compound 1 forms a monoclinic P lattice. The space group was found to be $P2_1/c$. The crystal structure of chiral compound **2** revealed two enantiomers cocrystallized in a triclinic lattice. The space group was found to be $P\bar{1}$. A disordered solvent molecule, CH_2Cl_2, was found in each unit cell. The presence of the solvent causes the two enantiomers inside the asymmetric unit to be slightly different. The inversion symmetry adds two more molecules to complete the unit cell. The whole cell consists of two pairs of enantiomers and one disordered CH_2Cl_2. Compound 3 also forms a monoclinic P lattice. The space group is $P\bar{1}$. Four solvent molecules, CH_2Cl_2, were found in a unit cell together with two chromophores. Compound 4 also forms cocrystals of two enantiomers in a monoclinic C lattice. The space group was found to be C2/c. The solved molecular structures are given in Figures 2−5.

For designing better metallocene chromophores, it is important to know whether cyclopentadiene (Cp) not directly linked

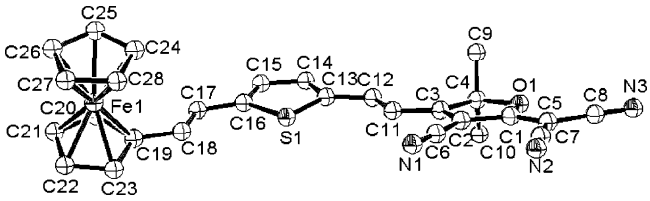

Figure 4. ORTEP labeling (50%) of **3**. (CCDC 249700. Some selected bond distances are listed in ref 16.)

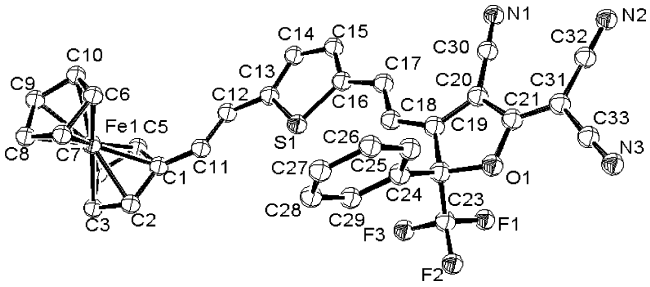

Figure 5. ORTEP labeling (50%) of **4**. (CCDC 249702. Some selected bond distances are listed in ref 16.)

Table 2. Average Bond Lengths (ABL) of the Two Cp Rings in **1**−**4**

compound	ABL of Cp1 (Å)	ABL of CP2 (Å)
1	1.417	1.407
2	1.416	1.391
3	1.425	1.417
4	1.413	1.411

to the bridge, significantly contributes to the electron-donating ability (i.e. whether the charge-transfer interaction passes through the metal). We examined the average bond length (ABL) of the two Cp rings of **1**−**4**. The Cp that is directly linked to the acceptor through the π bridge is labeled Cp1, and the other is labeled Cp2. The ABL of Cp2 is more sensitive than that of Cp1 toward the electron-withdrawing strength applied to the ferrocene. The ABL of the two Cp rings in **1**−**4** are listed in the Table 2. The ABL of Cp1 does not significantly change for **1**−**4**. The ABL of Cp2 clearly depends on the electron-withdrawing strength applied to the ferrocene, i.e. the strength and the distance of the acceptor. The stronger the electron-withdrawing strength on the ferrocene, the smaller is the ABL of Cp2. For example, the ABL of **2** is smaller than that of **1**, while the ABL of **1** is smaller than that of **3** because the acceptor is closer to the ferrocene in **1** than in **3**. Moreover, in all four chromophores the ABL of Cp1 is larger than Cp2. This evidence suggests that charge transfer interactions significantly pass through the iron to Cp2, suggesting that an improved design of Cp2 might improve NLO performance.

Strong nonlinear optical chromophores generally have large dipole moments leading to large dipole−dipole interactions between chromophores. Normally such strong interactions induce antiparallel packing that reduces the optical anisotropy of the bulk material. Hence, noncentrosymmetric crystals of strong NLO chromophores are rare. These intermolecular interactions are an important factor in determining the electrooptic efficiency in material.[10,17] In the four crystals, the neighboring chromophores align antiparallel; but the dimerization patterns are quite different.

Dimerization is one of the most important aspects of antiparallel packing of NLO chromophores. In a recent paper,

Wurthner, Wortmann, et al.[18] carefully examined the dimerization of merocyanine dyes. Centrosymmetric dimers formed in all the investigated merocyanines in concentrated solutions and in the solid state. Similarly, here all four Fc chromophores form dimers in the crystalline state with **1**, **2**, and **4** forming fully overlapped antiparallel dimers. The acceptor moiety of one molecule is adjacent to the Cp ring that links with the π bridge in the other molecule. Chiral compound **2** forms a centrosymmetric dimer of a pair of enantiomers. However, **4** forms a noncentrosymmetric dimer of the same enantiomers, which means there are two types of dimers with different chirality. The dimer of the S enantiomer is shown in Figure 6.

Compound **3** has a unique dimer structure (Figure 7). The acceptor group partially covers the thiophenyl ring rather than the Fc donor. For a simple model of a centrosymmetric dimer, see Scheme 2. The dimerization energy may be calculated from the equation[17] for two antiparallel dipoles

$$\Delta E_{\mathrm{dim}} = -\frac{N_{\mathrm{A}}}{4\pi\epsilon_0 d^3}\mu_{\mathrm{gM}}^2(1 - 3\cos^2\alpha)\sin^3\alpha \qquad (1)$$

where N_{A} is Avogadro's constant, ϵ_0 is the dielectric constant of the vacuum, d is the distance between planes, defined in Scheme 2, and α is the slip angle that results from the translational offset. For a given d, the absolute value of the dimerization energy increases as $\alpha \rightarrow \pi/2$. The distance between the two π planes in the dimer of **3** is about the same as that of the other three compounds ($d \approx 3.4$ Å). If only the electrostatic interaction is considered, the inclined dimer of **3** should be less stable than the fully overlapped conformation. Apparently, crystal packing forces dominate the electrostatic interaction between the dimers. It is not clear why only **3** forms this dimer structure.

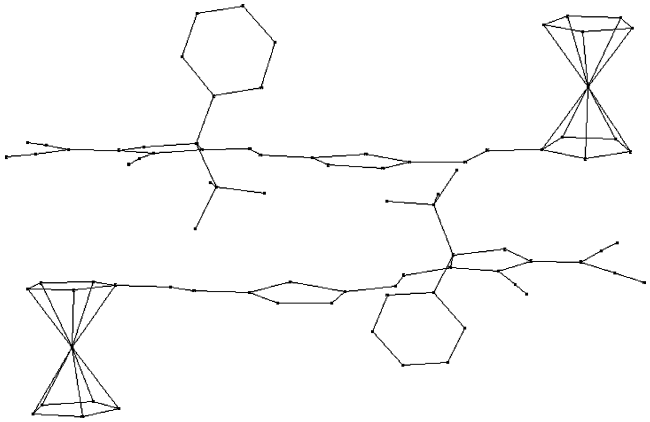

Figure 6. The asymmetric dimer of the S enantiomer of **4**.

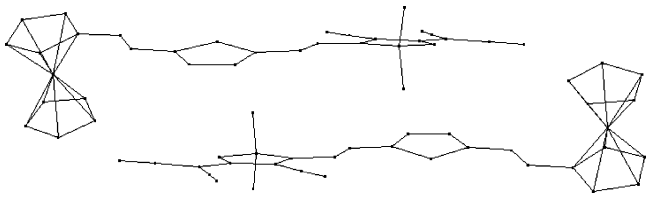

Figure 7. The dimer of **3**.

Scheme 2. Model for an Antiparallel Dimer of Two Dipoles.[17] (d is the distance between planes and α Is the Slip Angle that Results from the Translational offset.)

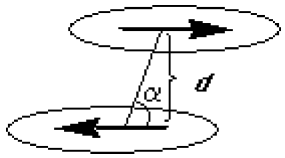

First Hyperpolarizabilities Measured by HRS. The first-order hyperpolarizabilities of **1**−**4** and *p*-nitroaniline (*p*NA) were measured by HRS using the solvent (chloroform) as internal reference. The excitation wavelength, $\lambda = 1000$ nm, was chosen to reduce the self-absorption of the scattered light by the chromophores and to minimize the impact of resonant enhancement on the measured hyperpolarizabilities. Self-absorption of the scattered light was of particularly importance in the case of **1**, where the low hyperpolarizability of this chromophore

(15) Barlow, S.; Bunting, H. E.; Ringham, C.; Green, J. C.; Bublitz, G. U.; Boxer, S. G.; Perry, J. W.; Marder, S. R *J. Am. Chem. Soc.* **1999**, *121*, 3715.

(16) Selected bond distances of **1** (Å) (Figure 2): Fe1−C4 2.017(5), Fe1−C2 2.021(5), Fe1−C6 2.027(5), Fe1−C7 2.027(5), Fe1−C3 2.031(5), Fe1−C1 2.032(4), Fe1−C8 2.032(5), Fe1−C10 2.036(5), Fe1−C5 2.038(5), Fe1−C9 2.040(5), O1−C15 1.331(5), O1−C16 1.494(4), N1−C19 1.141-(5), N2−C21 1.146(6), N3−C22 1.132(5), C13−C14 1.347(5), C13−C12 1.426(5), C13−C16 1.517(5), C14−C19 1.421(6), C14−C15 1.451(5), C3−C4 1.370(7), C3−C2 1.410(6), C1−C2 1.423(6), C1−C5 1.435(6), C1−C11 1.446(5), C16−C17 1.520(6), C16−C18 1.528(6), C15−C20 1.362(6), C11−C12 1.344(6), C21−C20 1.395(6), C5−C4 1.429(6), C20−C22 1.441(6), C10−C9 1.400(7), C10−C6 1.417(7), C8−C7 1.403(6), C8−C9 1.411(7), C7−C6 1.405(7). Selected bond distances of **2** (Å) (Figure 3): S enantiomer (the top molecule in Figure 3): Fe1−C13 2.019(6), Fe1−C20 2.036(6), Fe1−C18 2.038(5), Fe1−C12 2.039(5), Fe1−C16 2.045-(5), Fe1−C14 2.046(6), Fe1−C19 2.046(5), Fe1−C15 2.054(6), Fe1−C17 2.061(6), Fe1−C21 2.067(6), F1−C5 1.341(6), F2−C5 1.349(6), F3−C5 1.335(6), O1−C1 1.355(6), O1−C4 1.455(6), N1−C7 1.139(7), N2−C8 1.153(7), N3−C9 1.145(7), C1−C6 1.357(7), C1−C2 1.427(7), C2−C3 1.360(7), C2−C9 1.446(8), C3−C10 1.416(7), C3−C4 1.536(7), C4−C5 1.549(8), C6−C8 1.423(8), C6−C7 1.439(8), C10−C11 1.347(7), C11−C12 1.443(7), C12−C16 1.448(8), C12−C13 1.453(7), C13−C14 1.386-(7), C14−C15 1.405(8), C15−C16 1.415(7), C17−C21 1.406(7), C17−C18 1.410(7), C18−C19 1.399(7), C19−C20 1.424(7), C20−C21 1.432(7); R enantiomer (the bottom molecule in Figure 3): Fe2−C37 2.017(6), Fe2−C41 2.021(7), Fe2−C40 2.022(6), Fe2−C34 2.023(5), Fe2−C38 2.031-(6), Fe2−C33 2.033(6), Fe2−C39 2.033(6), Fe2−C42 2.033(7), Fe2−C35 2.034(5), Fe2−C36 2.041(5), F4−C26 1.330(6), F5−C26 1.339(6), F6−C26 1.336(6), O2−C22 1.352(6), O2−C25 1.457(6), N4−C28 1.148(7), N5−C29 1.136(7), N6−C30 1.148(7), C22−C27 1.335(7), C22−C23 1.448(7), C23−C24 1.379(7), C23−C30 1.437(8), C24−C31 1.425(7), C24−C25 1.537(7), C25−C51 1.522(7), C25−C26 1.530(8), C27−C29 1.442(8), C27−C28 1.445(8), C31−C32 1.340(6), C32−C33 1.438(7), C33−C37 1.419(7), C33−C34 1.425(7), C34−C35 1.419(7), C35−C36 1.415(8), C36−C37 1.402(8), C38−C39 1.370(9), C38−C42 1.400(9), C39−C40 1.397(8), C40−C41 1.370(9), C41−C42 1.417(10). Selected bond distances of **3** (Å) (Figure 4): Fe1−C22 2.034(3), Fe1−C21 2.037-(3), Fe1−C23 2.037(3), Fe1−C27 2.038(3), Fe1−C26 2.041(3), Fe1−C20 2.044(3), Fe1−C25 2.045(3), Fe1−C24 2.049(3), Fe1−C28 2.054(3), Fe1−C19 2.058(3), S1−C16 1.733(3), S1−C13 1.737(3), O1−C1 1.328(3), O1−C4 1.482(3), N1−C6 1.146(4), N2−C7 1.149(4), N3−C8 1.152(4), C1−C5 1.370(4), C1−C2 1.439(4), C2−C3 1.375(4), C2−C6 1.423(4), C3−C11 1.423(4), C3−C4 1.509(4), C4−C9 1.509(4), C4−C10 1.523(4), C5−C8 1.423(4), C5−C7 1.429(4), C11−C12 1.352(4), C12−C13 1.431(4), C13−C14 1.381(4), C14−C15 1.398(4), C15−C16 1.383(4), C16−C17 1.437(4), C17−C18 1.340(4), C18−C19 1.446(4), C19−C20 1.435(4), C19−C23 1.442(4), C20−C21 1.415(4), C21−C22 1.419(5), C22−C23 1.416(4), C24−C25 1.416(4), C24−C28 1.420(5), C25−C26 1.421(4), C26−C27 1.419(5), C27−C28 1.410(5). Selected bond distances of **4** (Å) (Figure 5): Fe1−C2 2.016(5), Fe1−C4 2.025(5), Fe1−C3 2.028(6), Fe1−C5 2.034(5), Fe1−C10 2.037(6), Fe1−C9 2.039(6), Fe1−C1 2.041(5), Fe1−C8 2.045(6), Fe1−C6 2.049(6), Fe1−C7 2.050(6), S1−C13 1.725-(5), S1−C16 1.728(5), F1−C23 1.346(5), F2−C23 1.340(5), F3−C23 1.351(6), O1−C21 1.347(6), O1−C22 1.461(6), N1−C30 1.168(7), N2−C32 1.165(7), N3−C33 1.158(8), C1−C2 1.417(7), C1−C5 1.429(7), C2−C3 1.413(8), C3−C4 1.395(9), C4−C5 1.409(7), C6−C10 1.389(8), C6−C7 1.411(9), C7−C8 1.413(9), C8−C9 1.426(9), C9−C10 1.415(8), C11−C12 1.336(7), C12−C13 1.443(7), C13−C14 1.387(7), C14−C15 1.380(7), C15−C16 1.385(7), C16−C17 1.437(7), C17−C18 1.354(7), C18−C19 1.413(7), C19−C20 1.390(7), C19−C22 1.519(7), C20−C30 1.402(8), C20−C21 1.444(7), C21−C31 1.352(7), C22−C24 1.493(7), C22−C23 1.525(8), C31−C32 1.422(8), C31−C33 1.442(9)

(17) Robinson, B. H.; Dalton, L. R. *J. Phys. Chem. A* **2000**, *104*, 4785−4795. Dalton, L. R.; Steier, W. H.; Robinson, B. H.; Zhang, C.; Ren, A.; Garner, S.; Chen, A.; Londergan, T.; Irwin, L.; Carlson, B.; Fifield, L.; Phelan, G.; Kincaid, C.; Amend, J.; Jen, A. K.-Y. *J. Mater. Chem.* **1999**, *9*, 1905−1920.

(18) Wurthner, F.; Yao, S.; Debaerdemaeker, T.; Wortmann, R. *J. Am. Chem. Soc.* **2002**, *124*, 9431.

Table 3. Relative Hyperpolarizability of **1**−**4** Measured by HRS

compound	**1**	**2**	**3**	**4**	*p*NA
$\beta/\beta_{\text{chloroform}}$	279 ± 31	450 ± 148	2633 ± 340	3333 ± 202	79 ± 7

necessitated the use of elevated chromophore concentrations. It has been demonstrated that high chromophore concentrations, leading to increasingly significant self-absorption, can attenuate the measured hyperpolarizability values.[19] Compound **1** demonstrates relatively modest extinction at 1000 and 500 nm; therefore, this excitation wavelength was chosen to minimize any attenuation of scattered light. Furthermore, for **1**, this excitation wavelength should provide minimal resonant enhancement, allowing for direct comparison to *p*NA. For compounds **2**−**4**, resonant enhancement may result in elevated β values. The extent of enhancement can be determined by measuring the excitation-wavelength dependence of the HRS intensity, and such experiments are currently underway. The details of the HRS experiment are provided in the Experimental Section.

The chromophore β values, reported relative to $\beta_{\text{chloroform}}$, can be converted to the absolute values using *p*NA as the standard. The β_{HRS} of *p*NA at 1064 nm in chloroform was measured by Shelton et al.[20] to be 22.7×10^{-30}esu. Using the relative β of the Fc chromophores, reported here, and a measured value of β_{HRS} *p*NA, the absolute values may be calculated (see Table 3).

DFT Calculations of the First Hyperpolarizability. DFT calculations were utilized to study the molecular hyperpolarizability. All calculations were performed with DMol,[3] a density functional code developed by Freeman, Delley, and co-workers.[21] Preliminary calculations using a variety of generalized gradient approximation (GGA) functionals on *p*-nitroaniline (*p*NA) showed that two of the most recent functionals, that of the Perdew, Burke, Ernzerhof[22] (PBE) and the revised version of this functional, the RPBE of Hammer, et al.,[23] gave results in excellent agreement with the MP2 calculations of Sim, et al.[24] In particular, Sim, et al., determined the dipole moment of *p*NA to be in the range 6.87−7.82 D, calculated with MP2 and their most extensive basis set, with variations in the calculated moment depending on whether the geometry of the (constrained) planar molecule was optimized with HF or MP2. Our calculations were done primarily with the PBE functional, with two structures being calculated with RPBE for comparison. Both the PBE and RPBE functionals yield β for pNA in excellent agreement with experimental gas-phase EFISH measurements.[25]

The energies and dipole vectors of a given molecule were calculated with zero field, together with 12 different field **E** settings of ±0.001 au and ±0.002 au along the three coordinate axes. Therefore, the polarizabilities so computed are ground-state properties of the molecule. No claim is made for the accuracy of DFT-based computations for properties, such as electronic transition frequencies, that are associated with the excited states. All calculations were spin restricted, as ferrocene is known to have spin zero. The DMol[3] code returns the energy and dipole vector for each field setting; the 13 dipole vectors were analyzed using the technique of Sim et al.[24] to extract the permanent dipole vector (the null field result), the polarizability, and the hyperpolarizability. The value of the angular averaged hyperpolarizability, measured by HRS, was calculated using the equations derived by Cyvin, Rauch, and Decius.[26]

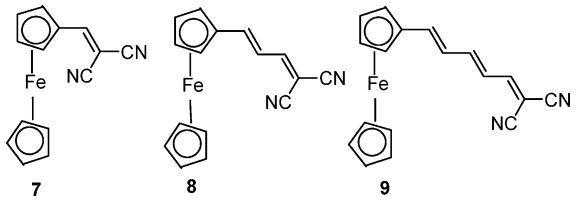

Dixon et al. calculated second-order hyperpolarizabilities of metallocenes using DFT .[27] The feasibility of calculating the first-order hyperpolarizability by DFT was verified by calculating the $\mu\beta$ and β_{zzz} of **7**−**9**, which were studied by Alain et al.[2b] who measured the $\mu\beta$ by electric-field-induced second-harmonic generation (EFISH). The results of our calculations are listed in Table 4. Our results showed that the DFT calculation of the Fc chromophores yielded lower $\mu\beta$ values than the experimental values (by a factor of approximately 3, in this series of Fc chromophores). This is at least partially due to the fact that DFT calculates the molecules in the gas phase while the experimental values were taken in the solution phase. In fact, the β value of pNA measured by EFISH in gas phase is 9.26×10^{-30} esu, while that in solution phase is 33.6×10^{-30} esu.[20,28] When the calculated values are compared with the experimental values of **7**−**9**, not only the trends but also the ratios of the hyperpolarizabilities are well predicted. This can best be seen by comparing the normalized values of experimental and calculated $\mu\beta$ and β_{zzz} in Table 4. Therefore, DFT calculations are suitable for systematically studying the present series of Fc chromophores.

We calculated both β_{HRS} and β_{zzz} using the molecular structures obtained from the X-ray analysis. These calculations have been done with the PBE/dnp Hamiltonian/basis set combination. The results are listed in Table 5. As mentioned above, due to the difference between the gas-phase and solution-phase β, directly comparing the DFT calculated values and the experimental values measured in solution is inappropriate. As a result we used pNA as a standard. We found that DFT calculated values for the first hyperpolarizabilities relative to pNA agreed well with the experimental values. (Table 5).

Because the crystal structures and hyperpolarizabilities of **1**−**4** are available, bond-length alternation (BLA) theory can be used to analyze the structure−property relationship for these molecules. It is arbitrary whether the two double bonds and one single bond in the TCF acceptor should be included in the analysis. In fact, we found that the differences between the bridge BLA and the acceptor BLA are very small for **1**, **2**, and **4**. Only in **3** is the bridge BLA (0.088 Å) significantly larger

(19) Pauley, M. A.; Wang, C. H.; Jen, A. K.-Y. *J. Chem. Phys.* **1995**, *102*, 6400.
(20) Kaatz, P.; Shelton, D. P. *J. Chem. Phys.* **1996**, *105*, 3918.
(21) Delley, B. DMol, a Standard Tool for Density Functional Calculations: Review and Advances. In *Modern Density Functional Theory: A Tool for Chemistry*; Seminario, J. M., Politzer, P., Ed.; Elsevier Science Publ.: Amsterdam, 1995; Vol. 2. DMol[3] is a product of Accelrys, Inc., San Diego, CA.
(22) Perdew, J. P.; Burke, K.; Ernzerhof, M. *Phys. Rev. Lett.* **1996**, *77*, 3865.
(23) Hammer, B.; Hansen, L. B.; Norskov, J. K. *Phys. Rev. B* **1999**, *59*, 7413.
(24) Sim, F.; Chin, S.; Dupuis, M.; Rice, J. E. *J. Phys. Chem.* **1993**, *97*, 1158.
(25) Davidson, E. R., Eichinger, B. E.; Robinson, B. H. Manuscript in preparation.
(26) Cyvin, S. J.; Rauch, J. E.; Decius, J. C. *J. Chem. Phys.* **1965**, *43*, 4083.
(27) Matsuzawa, N.; Seto, J.; Dixon, D. A. *J. Phys. Chem. A* **1997**, *101*, 9391.
(28) Kaatz, P.; Donley, E. A.; Shelton, D. P. *J. Chem. Phys.* **1998**, *108*, 849.

Table 4. Experimental and Calculated Hyperpolarizabilities of **7-9**

molecule	n[a]	experimental $\mu\beta/10^{-48}$ esu (normalized value[b])	DFT $\mu\beta/10^{-48}$ esu (normalized value[b])	DFT $\beta_{zzz}/10^{-30}$esu (normalized value[b])
7	1	92 (0.082)	28.6 (0.073)	4.18 (0.090)
8	2	420 (0.37)	125 (0.32)	16.5 (0.36)
9	3	1120 (1.0)	392 (1.0)	41.2 (1.0)

[a] Number of the double bonds in the bridge. [b] Values are normalized using the largest value in the corresponding column as 1.0.

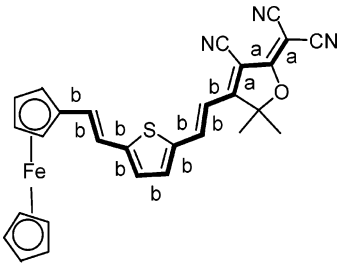

3

Figure 8. Bonds used for calculating BLA. (Highlighted bonds with label "b" are used for calculating the bridge BLA and "a" for acceptor BLA.)

Table 5. Experimental and DFT Calculated Data of **1**−**4**

	experimental β_{HRS}		DFT β_{HRS}		DTF β_{zzz}	
molecule	β/β_{CHCl3}	β/β_{pNA}	$\beta/10^{-30}$esu	β/β_{pNA}	$\beta/10^{-30}$esu	β/β_{pNA}
pNA	79 ± 7	1.0	3.08	1.0	7.20	1.0
1	279 ± 31	3.5	14.34	4.6	17.39	2.4
2	450 ± 148	5.7	14.75	4.8	26.66	3.7
3	2633 ± 340	33.3	110.1	35.7	82.34	11.4
4	3333 ± 202	42.4	134.1	43.5	318.1	44.2

Table 6. BLA Values of **1**−**4**

compound	bridge BLA (Å)	acceptor BLA (Å)	average BLA (Å)
1	0.092	0.097	0.095
2	0.091	0.092	0.091
3	0.088	0.067	0.078
4	0.076	0.073	0.074

than the acceptor BLA (0.067 Å). This might correlate with the unique dimerization conformation of **3** discussed above. The bonds used for calculating BLA are shown in Figure 8. The bridge BLA, the acceptor BLA, and the average BLA are listed in Table 6. The BLA values were compared with hyperpolarizability β_{zzz} calculated by DFT as described below.

The correlation between the hyperpolarizabilities and BLA of **1**−**4** was studied. The bridge BLA was used to avoid the effect of dimerization discussed above. Because the BLA is related to the bonds along the long axis of the molecule, theoretical values of β_{zzz} in Table 6 were used. A linear relationship is obtained (Figure 9). A quasi-linear relationship between β_{zzz} and BLA values over the range from 0.05 to 0.1 Å was predicted by Marder et al. more than 10 years ago and has since been a guide for designing nonlinear optical chromophores.[29] However, because of the difficulty of obtaining crystals suitable for X-ray analysis, the previous systematic studies were based on calculated BLA values. Also, the strengths of donor and acceptor groups were modeled by an external field.[30] Our results showed that in a well-designed system, such a linear relationship does exist even when chromophores with different acceptors are compared.

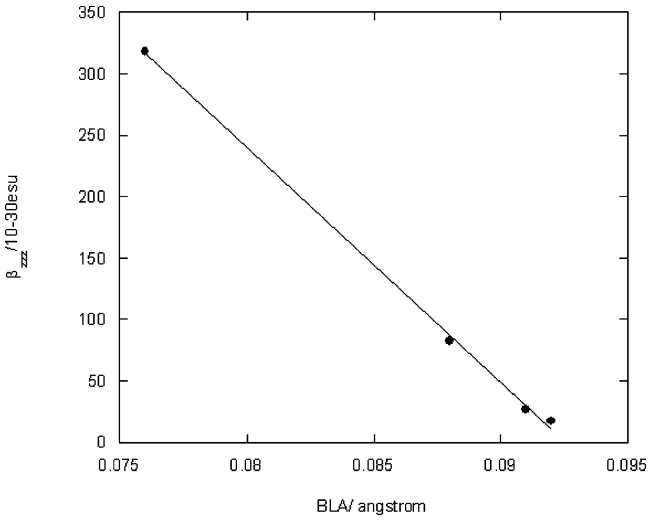

Figure 9. Linear relationship between BLA and first-order hyperpolarizability. (The data are fit by a linear equation of $\beta_{zzz} = 19.1 \times (0.0925\text{-BLA}) \times 10^{-27}$ esu with a linear correlation coefficient of $R = 0.9993$.) The data lie within the region of linearity predicted by Marder et al.

The molecular structure of **4** is unique: In **1**−**3**, all the ene structures adopt a trans conformation (as expected). While in **4**, the diene structure C17−C18−C19−C20 has a cis conformation (Figure 5). To understand whether this is due to the crystal packing, we calculated the energies of cis and trans conformations in the gas phase with DMol3. In both cases, optimized geometries were used. Indeed, the cis conformation is 25.4 kcal/mol more stable than the trans conformation. For comparison, cis and trans conformations of **3** were also calculated. In this case, the trans conformation is 22 kcal/mol more stable. Our results are consistent with the crystal structure. This suggests that the cis conformation of **4** is not solely the result of crystal packing forces.

Electrooptic Property. Compound **4**, with a strong acceptor, a long bridge, and a chiral center, is expected to have a large electrooptic coefficient. A guest−host system of **4** in amorphous polycarbonate (APC) with 20 wt % loading was prepared by spin-coating a solution of **4** and APC in cyclopentanone on a glass slide possessing an indium−tin-oxide (ITO) overlayer. The samples were spin-coated at a spread speed of 500 rpm and a 20 s spin at 700 rpm. The film was then baked overnight at 85 °C. The film was contact poled between the temperatures of 140 °C and 150 °C at 1.0 MV cm^{-1} for 5 min. The resulting r_{33} value was 25 pm V^{-1} at 1300 nm. For comparison, a guest−host system of **3** was also prepared and poled at the same condition. An r_{33} of 5 pm V^{-1} was obtained at 1300 nm. The poling conditions consisted of a current of 2 μA for **3** and 11−14 μA for **4**. Because the weight loading is the same and **3** has a smaller molecular weight than **4**, the film of **3** contained a higher concentration of Fc groups. The result shows that, at least in this case, the organometallic species did not cause any unusual conduction problems in the poling process.

(29) Marder, S. R.; Gorman, C. B.; Tiemann, B. G.; Cheng, L.-T. *J. Am. Chem. Soc.* **1993**, *115*, 3006.
(30) Marder, S. R.; Gorman, C. B.; Meyers, F.; Perry, J. W.; Bourhill, G.; Bredas, J.-L.; Pierce, B. M. *Science* **1994**, *265*, 632.

To the best of our knowledge, there is only one previously reported value of r_{33} for an organometallic chromophore in a poled film. In that work, incorporation of 1-ferrocenyl-4-*E*,*E*-(4-nitrophenyl)butadiene into poly(methyl methacrylate) at 2% molar loading (0.19 mmol g^{-1}) yielded an $r_{33} = 0.8$ pm V^{-1} measured at 820 nm. The loading of **4** is 20 wt % corresponding to a loading density of 0.32 mmol·g^{-1}. The molar loading density is only 68% higher than the previous one, while the electrooptic coefficient is more than 30 times higher. Such large increases could be due to a combination of high hyperpolarizability of the chromophore, good compatibility with the polymer matrix, and optimized poling condition.

The resulting r_{33} is comparable to values recently reported,[11,31] using chromophores containing bulky side groups designed to prevent aggregation.[17,32] However, this strategy has a drawback in that it limits the loading density. Compound **4** achieved a high r_{33} at 20 wt % loading in the absence of bulky substituents. The electrooptic efficiency may be further increased by adding periphery structures, optimizing loading density, choosing a more compatible polymer matrix, or linking the chromophore to a polymer backbone.[17]

Experimental Section

General. All commercially available compounds were used as supplied. Tetrahydrofuran, dichloromethane, and diethyl ether were distilled over drying agents under nitrogen before use. 2-Dicyanomethylene-3-cyano-4-methyl-5-dimethyl-2,5-dihydrofuran (**5**), 4,4,4-trifluoro-3-hydroxy-3-phenyl-2-butanone (the precursor of **6**), and [(1*E*)-2-(5-formyl-2-thienyl)ethenyl]ferrocene (**8**), were synthesized following literature methods.[8,12,13] UV−visible spectra were recorded on a SHIMADZU 1601 UV spectrometer. ^{1}H NMR spectra were recorded on a Bruker AM-300. Crystals of **1**−**4**, suitable for X-ray diffraction analysis, were obtained by slow diffusion of a heptane layer to a concentrated solution of the corresponding chromophore in dichloromethane. Prevalere Life Sciences, Inc., performed all elemental analyses.

Hyper-Rayleigh Scattering Measurement. Hyper-Rayleigh scattering (HRS) measurements were performed to quantify the first hyperpolarizability (β) of **1**−**4**, and *p*NA. Solutions were prepared in chloroform (Fisher: ACS Spectranalyzed). The concentrations employed were as follows: **1** (23 μM), **2** (939 nM), **3** (348 and 697 nM) **4** (220 and 330 nM), pNA (173 and 346 μM).

A mode-locked Ti:sapphire oscillator (Spectra-Physics Tsunami) provided excitation at 1000 nm, consisting of 100-fs pulses (full-width at half-maximum, fwhm), an 80 MHz repetition rate, and 550 mW of incident power. The laser spectrum (fwhm $\approx$ 12 nm) was monitored throughout the experiment. The incident light was focused into the middle of a low-volume flow cell connected to an in-line 0.1-μm PTFE filter. Scattered light was imaged onto the slits of a spectrograph (Acton 300i) through a 700-nm short-pass filter and a piece of blue-green BK7 glass. Detection was accomplished with a 1340 × 100 pixel, red-edge enhanced, back-thinned, LN_2-cooled CCD camera (Roper Scientific), using exposure times of 240−500 s. A more detailed discussion of the experimental apparatus is described elsewhere.[33]

HRS was confirmed by a quadratic dependence of the signal intensity on incident power. Furthermore, the spectral-width of the HRS peak was equal to the incident field and tracked with changes in excitation wavelength. Signal amplitudes were monitored for consistency over the course of successive scans to monitor the onset of bulk photodegradation. No measurable photodegradation was observed during these experiments. Additionally, solution concentrations were carefully chosen to avoid self-absorption of the scattered light by the chromophores. No measurable self-absorption effects were observed at the concentrations employed.

Data were analyzed in the MATLAB environment by fitting the HRS emission peaks to a Gaussian functional form to determine the intensities. Intensities were converted to β by comparing spectra of the sample solutions to corresponding spectra of neat chloroform. β values are expressed relative to β_{CHCl3}, as determined through the following equation (where I is the signal intensity and N is the number density):

$$\frac{I_{\text{sample}}}{I_{\text{solvent}}} = \frac{N_{\text{sample}}\langle\beta^2_{\text{sample}}\rangle + N_{\text{solvent}}\langle\beta^2_{\text{solvent}}\rangle}{N_{\text{solvent}}\langle\beta^2_{\text{solvent}}\rangle} = \left(\frac{N_{\text{sample}}}{N_{\text{solvent}}}\right)\frac{\langle\beta^2_{\text{sample}}\rangle}{\langle\beta^2_{\text{solvent}}\rangle} + 1$$

Synthesis. 2-Dicyanomethylene-3-cyano-4-methyl-5-phenyl-5-perfluoromethyl-2,5-dihydrofuran (6).[13] In a 25 mL round-bottom flask were mixed 1.8 g of 4,4,4-trifluoro-3-hydroxy-3-phenyl-2-butanone (8.25 mmol), 1.16 g of malonitrile (17.6 mmol), and 1 mL of absolute ethanol. The mixture was heated in a microwave reactor for 1 h at 35 W. The reaction temperature was measured by an internal thermometer to be between 95 and 100 °C. After the reaction, a couple of drops of water were added to quench the reaction. The crude product was purified by chromatography on silica gel with CH_2Cl_2 as the eluant to yield 1.1 g of **6** (42% yield). ^{1}H NMR δ ($CDCl_3$): 7.58−7.54 (3H, m), 7.45−7.41 (2H, m), 2.48 (3H, s). MS (ESP): 338.05 (M + Na).

Chromophore 1. Into a mixture of 16 mL of $CHCl_3$ and 4 mL of THF were dissolved 0.37 g of ferrocenecarboxaldehyde (1.7 mmol) and 0.50 g of **5** (2.5 mmol) . To this mixture was added three drops of triethylamine. The solution was refluxed overnight and then concentrated under reduced pressure. The residue was chromatographed on silica gel using 1:3 hexane/ethyl acetate as the eluant. The yield was 0.38 g (57% yield). ^{1}H NMR δ ($CDCl_3$): 7.68 (1 H, d, J = 15.4 Hz), 6.50 (1 H, d, J = 15.4 Hz), 4.85 (2 H, t, J = 1.8 Hz), 4.70 (2 H, t, J = 1.8 Hz), 4.25 (5 H, s), 1.74(6 H, s). HRMS (ESP): 396.0800 (M + H), 418.0613 (M + Na). Anal. Calcd for $C_{22}H_{17}FeN_3O$: C, 66.86; H, 4.34; N, 10.63. Found: C, 66.52; H, 4.54; N, 10.56.

Chromophore 2. Into about 0.5 mL of CH_2Cl_2 were dissolved 0.1 g (0.317 mmol) of **6** and 0.067 g (0.313 mmol) of ferrocenecarboxaldehyde. To this mixture was added 2 mL of ethanol. The mixture was heated at 60 °C for 1 h (or left at room temperature overnight). After cooling to room temperature, the mixture was concentrated to about 1 mL. The crystalline precipitate was collected and washed with a little ethanol. The crude product was recrystallized in a mixture of heptane and dichloromethane to yield 116 mg of pure product (72% yield). ^{1}H NMR δ ($CDCl_3$): 7.64 (1 H, d, J = 15.5 Hz), 7.44−7.61 (5 H, m), 6.53 (1 H, d, J = 15.5 Hz), 4.90 (2 H, s, br), 4.63(2 H, s, br), 4.16, (5 H, s). HRMS (ESP): 534.0485 (M + Na). Anal. Calcd for $C_{27}H_{16}F_3FeN_3O$·0.25(CH_2Cl_2): C, 61.46; H, 3.12; N, 7.89. Found: C, 61.94; H, 3.48; N, 7.95.

Chromophore 3. In a mixture of 16 mL of $CHCl_3$ and 4 mL of THF were dissolved 0.40 g of **8** (1.2 mmol) and 0.40 of **5** (2.0 mmol). To this mixture was added three drops of triethylamine. The solution was refluxed overnight and then concentrated under reduced pressure. The residue was chromatographed on silica gel using 1:1 hexane/ethyl acetate as the eluant. The yield was 0.51 g (84% yield). ^{1}H NMR δ ($CDCl_3$): 7.76 (1 H, d, J = 14.7 Hz), 7.31 (1 H, d, J = 4.0 Hz), 6.93−6.95 (2 H, m), 6.78 (1 H, d, 16.0 Hz), 6.59 (d, J = 14.7 Hz), 4.58 (2 H, s, br), 4.50 (2 H, s, br), 4.23 (5 H, s), 1.75 (6 H, s). HRMS (ESP): 503.0740 (M + H), 526.0638 (M + Na). Anal. Calcd for $C_{28}H_{21}FeN_3OS$: C, 66.81; H, 4.20; N, 8.35. Found: C, 66.75; H, 4.44; N, 8.44.

Chromophore 4. In about 0.5 mL of CH_2Cl_2 were dissolved 0.1 g (0.310 mmol) of **8** and 0.1 g (0.317 mmol) of **6**. To this mixture was added 2 mL of ethanol. The mixture was heated at 60 °C for 1 h (or

(31) For recent reviews: Dalton, L. R.; Robinson, B. H.; Jen, A. K.-Y.; Steier, W. H.; Nielsen, R. *Opt. Mater.* **2003**, *21*, 19. Ma, H.; Jen, A. K.-Y.; Dalton, L. R. *Adv. Mater*. **2002**, *14*, 1339.
(32) Ma, H.; Chen, B.; Sassa, T.; Dalton, L. R.; Jen, A. K.-Y. *J. Am. Chem. Soc.* **2001**, *123*, 986.
(33) Firestone, K. A.; Reid, P. J.; Lawson, L. R.; Jang, S.-H.; Dalton, L. R. *Inorg. Chim. Acta.* **2004**, *357*, 3957−3966.

left at room temperature overnight). After cooling to room temperature, the mixture was concentrated to about 1 mL. The crystalline precipitate was collected and washed with a little ethanol. The crude product was recrystallized in a mixture of heptane and dichloromethane to yield 146 mg of pure product (76%). ^{1}H NMR δ ($CDCl_3$): 7.77 (1 H, d, J = 15.0 Hz), 7.50−7.56 (5 H, m), 7.27 (1 H, d, J = 3.6 Hz), 7.01 (1 H, d, J = 16.1 Hz), 6.95 (1 H, d, J = 3.5 Hz), 6.75 (1 H, d, J = 15.0 Hz), 6.65 (1 H, d, J = 16.1 Hz), 4.54 (2 H, s, br), 4.50 (2 H, s, br), 4.20 (5 H, s). HRMS (ESP): 642.0508 (M + Na). Anal. Calcd for $C_{33}H_{20}F_3FeN_3OS\cdot0.6(CH_2Cl_2)$: C, 60.20; H, 3.19; N, 6.27. Found: C, 60.11; H, 3.66; N, 6.05.

Acknowledgment. Support from the Air Force Office of Scientific Research, the Office of Naval Research and the National Science Foundation are gratefully acknowledged.

Supporting Information Available: X-ray crystallographic files in CIF format with the coordinates of molecules **1**−**4**. This material is available free of charge via the Internet at http://pubs.acs.org.

JA0449123